

알제리 Pinus Halepensis Tannin Foam을 이용한 수용액에서의 Cr(VI) 흡착

Zeyneb Hamadi^{*,**,*†}, Rabah Chaid^{*}, Mohammed Kebir^{*****}, Siham Amirou^{****},
Hisham Essawy^{*****}, and Antonio Pizzi^{****}

^{*}Faculty of engineering, Research Unit Materials, Processes and Environment URMPE,
University M'hamed Bougara of Boumerdes/FSI

^{**}Research Unit on Analysis and Technological Development in Environment (URA-DTE/ CRAPC)

^{***}Laboratory of Reaction Engineering, FGMGP/USTHB

^{****}LERMAB, University of Lorraine

^{*****}Department of Polymers and Pigments, National Research Centre

(2020년 1월 5일 접수, 2020년 3월 19일 수정, 2020년 3월 25일 채택)

Adsorption of Cr(VI) from Aqueous Solutions Using Algerian Pinus Halepensis Tannin Foam

Zeyneb Hamadi^{*,**,*†}, Rabah Chaid^{*}, Mohammed Kebir^{*****}, Siham Amirou^{****},
Hisham Essawy^{*****}, and Antonio Pizzi^{****}

^{*}Faculty of engineering, Research Unit Materials, Processes and Environment URMPE, University M'hamed Bougara of
Boumerdes/FSI, Frantz Fanon City, Indépendance Avenue 35000 Boumerdes, Algeria

^{**}Research Unit on Analysis and Technological Development in Environment (URA-DTE/ CRAPC),
BP 384, 42000 Bou-Ismaïl, Tipaza, Algeria

^{***}Laboratory of Reaction Engineering, FGMGP/USTHB, BP 32, 16111 Algiers, Algeria

^{****}LERMAB, University of Lorraine, EA 4370, 27 rue Philippe Séguin, BP 21042, 88051 Epinal cedex 9, France

^{*****}Department of Polymers and Pigments, National Research Centre, Dokki 12622, Cairo, Egypt

(Received January 5, 2020; Revised March 19, 2020; Accepted March 25, 2020)

Abstract: In this study, new adsorbent tannin foam was prepared from Algerian natural pinus halepensis tannin (APTF). The prepared material has been used as an efficient and environmentally friendly adsorbent to remove chromium (Cr(VI)), which is considered as the most toxic pollutant in wastewater. The different features of the adsorbent in terms of the structural and morphological characteristics were studied. The impact of different factors on the adsorption process, such as pH, adsorbent mass, initial Cr(VI) concentration, and temperature, was investigated. The data obtained from the Cr(VI) adsorption revealed an improvement of the removal efficiency with increasing the adsorbent dose, the pH had a notable effect on Cr(VI) adsorption capacity, whereas the effectiveness decreased by rising the initial metal concentration. In addition, it was observed that adsorption efficiency enhanced with increasing temperature, indicating that the adsorption was endothermic and spontaneous in nature. Moreover, the results were best represented by the pseudo-second order kinetic model and the Langmuir isotherm model ($q_m = 400 \text{ mg} \cdot \text{g}^{-1}$) at 293 °K and pH ~2.

Keywords: adsorption, foam, Cr(VI), isotherms, kinetics.

Introduction

Recently, issues of water pollution has recently gained great concern worldwide. Thus, coping with the pollution problems

of water while securing sufficient supply of clean water for human consumption constitutes a great challenge from scientific point of view.¹ The presence of emerging contaminants such as hexavalent chromium (Cr(VI)) is considered as a definite carcinogenic hazard either by oral or dermal absorption. Inhalation can also be a reason for cancer in lungs as well as in the digestive tract, epigastric pain, nausea, vomiting, severe

[†]To whom correspondence should be addressed.
ze.hamadi@univ-boumerdes.dz, ORCID[®]0000-0002-3454-5303
©2020 The Polymer Society of Korea. All rights reserved.

diarrhea and hemorrhage in many cases especially for persons exposed frequently to an adequate airborne concentration.² The ejection of these compounds into the aquatic environment can cause death of all living organisms. Various materials are conventionally dedicated for the purpose of water treatment, including activated carbon, activated sludge and technologies processes like advanced oxidation, reverse osmosis membranes and nano filtration. Nevertheless, these techniques are not much effective for treatment in case of complicated water compromising different categories of pollutants such as metals, surfactants, personal care products, industrial additives and pharmaceutical compounds.

In this context, among the major effective processes of treatment comes the adsorption technique, which has a distinct advantage over the other techniques due to its easier and practical use in aqueous media. The nature of an adsorbent plays a key role in any adsorption technique. The focus on low cost adsorbents, formulated preferably from natural substances and local waste, while exhibiting high performance, has been explored by many researchers.³ Tannins are inexpensive, natural substances that can be easily extracted from plants. As they are principally rich in adjacent phenolic hydroxyls, they have a high affinity for complexing metal ions.^{4,5} A reasonable number of previous studies have drawn the attention to the efficacy of adsorbents fabricated from tannins in the removal of a wide range of pollutants such as dyes,⁶ microorganisms,⁷ surfactants⁸ and heavy metal ions.⁹⁻¹³ Rigid tannin foams have been recognized for some time, but their utilization as adsorbents has just been explored few years ago.^{9,14} Rigid tannin foams are mainly formulated from commercial tannin extracts, such as Quebracho (*Schinopsis balansae*), Mimosa (*Acacia mearnsii*) or Pine (*Pinus pinaster*). This study focus on the exploration of constructing rigid tannin foams from Pine (*Pinus halepensis*) bark tannin and employing them as adsorbents. *Pinus halepensis* is one of the important forest species in the Mediterranean basin. It covers over 900000 hectares in Algeria alone.¹⁵ Great responsiveness for the exploitation of Mediterranean pine forests is intended for wood production. Thus, using Algerian *pinus halepensis* bark as a raw material for foam production is meaningful issue to be considered. The foam is basically prepared under acidic conditions while making use of furfuryl alcohol as a crosslinking agent and diethyl ether as a foaming agent.^{14,16} Several characterization techniques are devoted for the characterization of the foam including Fourier transform infrared (ATR-FTIR), thermogravimetric analysis (TGA) and scanning electron microscopy (SEM). Fur-

thermore, the foams were evaluated for their potential applicability as efficient adsorbent for Cr(VI) elimination from aqueous solutions. The study is extended to several different influences on the adsorption process, such as contact time, pH, adsorbent dose, initial Cr(VI) concentration, and temperature. In addition, adsorption kinetics, thermodynamic parameters, and isothermal characteristics of the adsorption process at equilibrium were also studied.

Experimental

Materials. The *pinus halepensis* bark was collected from the forest of Boumerdes region, north Algeria. The barks were air-dried and crushed in a mill and screened to a particle size below 500 μm . Methanol (CH_3OH ; 99.8% purity), folin reagent ($\text{C}_{10}\text{H}_5\text{Na}_3\text{OS}$; 97% purity) reagent (1/10; v/v in demineralized water), sodium carbonate (Na_2CO_3 ; 99% purity) solution (0.7 M), sodium sulfite (Na_2SO_3 ; 98.5% purity), sodium bisulfite (NaHSO_3 ; 35% purity), formaldehyde (CH_2O ; 37% purity), hydrochloric acid (HCl; 37% purity), furfuryl alcohol ($\text{C}_5\text{H}_6\text{O}_2$; 98% purity), glyoxal ($\text{C}_2\text{H}_2\text{O}_2$; 40% in water), diethyl ether in analytical purity grade 99.5%, *p*-toluenesulfonic acid (PTSA; 98% purity), potassium dichromate ($\text{K}_2\text{Cr}_2\text{O}_7$; 99% purity) and sodium hydroxide (NaOH; 98% purity) were all supplied from Sigma-Aldrich Chemical Co.

Preparation of the Adsorbent (APTF). The extraction of tannins was carried out in water using the reagents NaOH, Na_2SO_3 and NaHSO_3 at 80 °C for 120 min, while the liquid to solid ratio of the sample in the aqueous phase was fixed at L/S=8.¹⁷ The extraction was carried out in triplicate. Sodium hydroxide (NaOH) was used to improve the extraction yield whereas the sodium sulphate (Na_2SO_4) and sodium bisulphite (NaHSO_3) were used to decrease and stabilize the viscosity of the extract. Afterward, the supernatant was filtered using Whatman filter paper (No. 1, 0.45 μm) and the residue was washed with distilled water. Finally, the extract was evaporated at reduced pressure on a rotary evaporator and subsequently lyophilized. The obtained extract was used to preparing pine foam.

A standard recipe for pine foam preparation has been described previously with some modifications.¹⁸ In brief, 30 g of the extracted pine bark tannin was mixed with water (6 g) and furfuryl alcohol (19 g). Then, glyoxal (7.4 g) was added as additional crosslinking agent. Continuous shaking of the mixture was conducted until a homogeneous liquid was ensured. After that, 1 g of diethyl ether was added as a foaming agent.

At last, 11 g of *p*-toluenesulfonic acid (pTSA) solution (65% (w/v) of mass of PTSA dissolved in distilled water volume) was added as a catalyst. The foams were evolved in few minutes after adding the catalyst. The foams were then divided into small pieces and cured for 24 h to remove any residual solvent. Subsequently, grinding was undertaken to convert them into the powder form in order to maximize the surface area. The adsorbent derived from pine tannin foam (APTF) was washed to remove any remaining un-reacted reagents and eventually dried at 60 °C.

Characterization Methods. FTIR spectroscopic analysis was scanned in the wavelength range 4000-400 cm⁻¹ at a resolution of 4 cm⁻¹ for investigation of the chemical functionality of the tannin pine bark and characteristics of the adsorbent using Bruker Alpha Spectrum equipped with ATR-FTIR module.

The thermal analysis was performed on TA instrument (TGA Q50 instrument). The temperature run covered the range from 25 to 600 °C at a heating rate of 10 °C/min under air flow of 40 mL/min.

The morphology of the APTF adsorbent was examined before and after Cr(VI) adsorption using field emission scanning electron microscopy (FE-SEM, HITACHI S-4700) operated at 20 kV acceleration voltage.

The point of zero charge of APTF (PZC) is the pH of the aqueous solution in which the solid exists under neutral electric potential, which can be identified using the experimental protocol described by Lopez-Ramon *et al.*¹⁹ Flasks of NaCl solutions (0.1 M) with pH values between 2 and 10, normally adjusted with 0.01 M solutions of HCl or NaOH, were prepared. 0.5 g of the adsorbent was mixed with 20 mL of each solution separately and stirred for 48 h before filtration. The pH values of the resulting solutions were then recorded and plotted as a function of the initial pH for each solution. The PZC corresponds to the pH of the solution at which the lines meet at the common point of intersection.

Adsorption Study of Hexavalent Chromium(Cr(VI)) Ions. A series of Cr(VI) solutions were obtained at different concentrations ranging from 50 to 300 mg/L by conducting dilution of K₂Cr₂O₇ stock solution (1000 mg/L). The adsorption studies were carried out using a known amount of APTF as adsorbent, thoroughly mixed at 120 rpm with 100 mL of defined concentrations of Cr(VI) at different pH and temperature values. The pH of the reaction mixture was initially regulated using HCl (0.1 M) or NaOH (0.1 M). The aliquots were withdrawn at definite interval times, then filtered and the remaining Cr(VI) concentration in the solution was estimated

using the analytical Jena 210 Specord spectrophotometer at $\lambda_{\max} = 350$ nm. The variables of the experimental conditions can be summarized as the initial concentration of Cr(VI) (50-300 mg/L), pH (2-9), the adsorbent dose (0.1-2 g/L) and the contact time (5-2880 min). For the purpose of optimization of adsorption conditions, a given parameter has been changed while the others were kept constant. The adsorption capacity at equilibrium, Q_e (mg/g) and removal efficiency, A (%) are represented using eqs. (1) and (2):

$$Q_e = \frac{(C_0 - C_e)V}{m} \quad (1)$$

$$A(\%) = \frac{(C_0 - C_e)}{C_0} \times 100 \quad (2)$$

Where, Q_e : is the adsorption capacity (mg/g), V : is the volume of the solution (L), C_0 and C_e : are the initial and equilibrium concentration of Cr(VI) (mg/L) and m : is the mass of adsorbent (g).

Results and Discussion

Characterization of the Adsorbent. The spectra of the adsorbent were compared with the IR spectrum of the raw tannin as revealed in Figure 1(a). Generally, the wide bands in the range of 3200-3600 cm⁻¹ are attributed to the OH stretching vibration. Small peaks near 2900 cm⁻¹ can be identified in all spectra, due to the aromatic C-H stretching vibrations. The bands at 1441 and 1650 cm⁻¹ are characteristic of aromatic (-C=C-).¹⁷ The peaks appearing at 1602, 1514 and 1441 cm⁻¹ are assigned to the stretching vibration of the aromatic rings (-C=C-).²¹ It is obvious that the 1254 cm⁻¹ band refers to the B-cycle catechetal vibration band present in fisetinidins and catechins.²¹⁻²³ Additionally, the spectrum of the foam indicates the presence of ionizable functional groups (i.e. carboxyl, hydroxyl) that are able to interact with metal ions. The FTIR spectra collected for the APTF before and after adsorption of Cr(VI) ion are demonstrated in Figure 1(b). It is interesting to notice that after adsorption of the Cr(VI) ion, there was a backward shift of the original characteristic OH stretching vibration from 3277 to 3117 cm⁻¹. This perturbation suggests the emergence of new interaction between Cr(VI) ions and the hydroxyl groups containing sites of the adsorbent.

The thermal gravimetric profile (TG-DTA) of the adsorbent, performed under air atmosphere, is displayed together with its derivative curve as well as DTA profile in Figure 2(a) and 2(b), respectively. It shows that the degradation of pinus helpensis

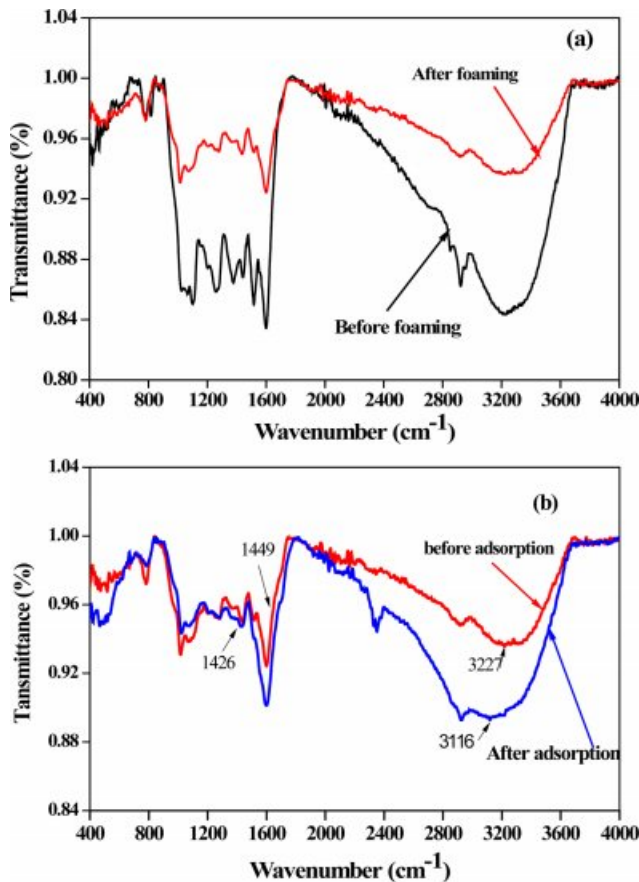


Figure 1. FTIR spectra (a) pinus tannin before and after foaming reaction; (b) APTF material before and after adsorption.

foam takes place in the course of four stages. A first loss of the mass is observed at about 100 °C, which is attributed to the elimination of residual water (almost 12%). The DTA thermogram shows that the first step is endothermic. The decomposition proceeds only after absorption of a definite amount of thermal energy that initiates the modification process by breaking the molecular chains. This result has already been described by Moubarik.²⁰ The second step (observed at a temperature range between 125 and 231 °C) is exothermic as indicated by the DTA and corresponds to a mass loss about 24% and can be attributed to a partial decomposition with oxidation of the intermolecular bonds. The third degradation step took place between 231 and 430 °C, which signifies the decomposition of the aromatic nuclei of the tannin foam.²¹ The fourth step (430–600 °C) refers to the oxidation of the residues. The DTA analysis confirmed all steps proceeding above 200 °C are exothermic reactions. Accordingly, it can be concluded that the adsorbent APTF is thermally stable. The thermal behavior of

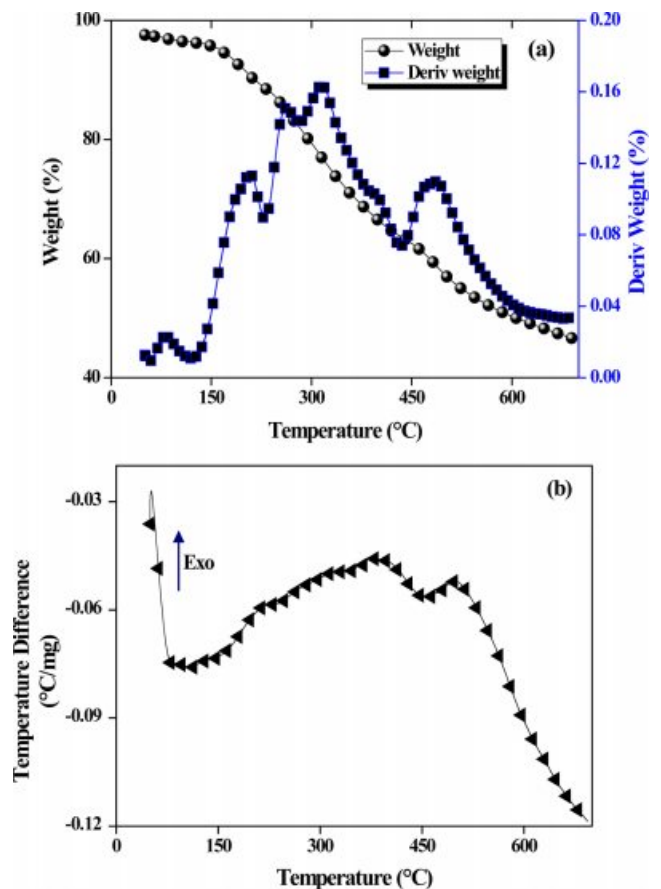


Figure 2. Thermal analysis of APTF: (a) thermogravimetric analysis (TGA) and the relevant derivative for APTF adsorbent; (b) differential temperature thermogram (DTA) of APTF adsorbent.

the adsorbent has depends essentially on the nature of the tannin, the type of intermolecular bonds and the rigidity of the foam structure.

The imaging with SEM was done to identify the morphological features of the adsorbent surface specially any change occurred on the APTF after Cr(VI) adsorption (Figure 3). It is initially clear that the material exhibits porosity in the form of cavities, which have been most likely resulting by the presence of the foaming agent during the foaming stage (Figure 3(a) and 3(b)). After adsorption of the chromium ions, the surface of APTF became smoother and encountered overlap due to Cr(VI) adsorption (Figure 3(c) and 3(d)).

Effect of pH on Adsorption. For any adsorption process, the solution pH is an essential parameter that can affect the interaction between the adsorbent and the adsorbate. The adsorption of Cr(VI) was studied as a function of pH at 20 °C. As such, 0.04 g of APTF was added to 100 mL (0.4 g/L) to give 100 mg/L solution of Cr(VI) while the pH was adjusted

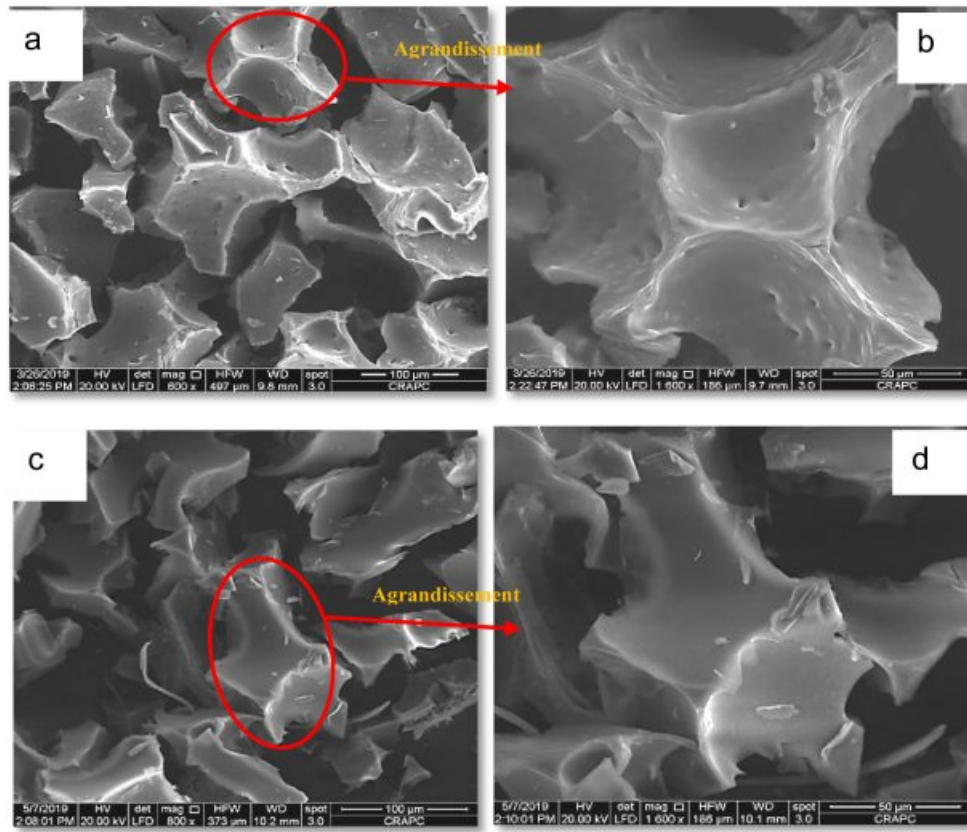


Figure 3. Scanning electronic microscopy (SEM) imaging of APTF: (a, b) before adsorption; (c, d) after adsorption.

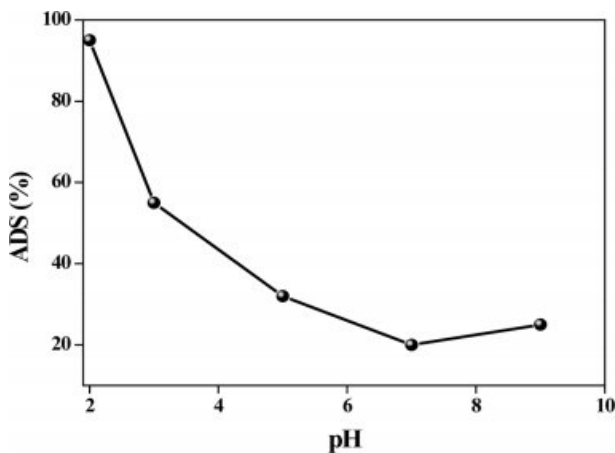


Figure 4. Variation of Cr(VI) adsorption onto APTF as a function of pH.

to different values ranging from 2 to 9. The adsorption capacity was determined after 2 h of contact (Figure 4). It has been found that the highest adsorption capacity of APTF was reached at $\text{pH} \sim 2$. In addition, a decrease of adsorption capacity was attained while increasing the pH from 2 to 9. Very low

adsorption capacities were observed at pH values above 9. This is related to the nature of surface charge of the adsorbent and the different complexes that Cr(VI) can form in aqueous solutions over different pH values. To understand that more deeply, it was necessary to find out the point of zero charge (PZC). A plot of the $(\text{pH}_{\text{initial}} - \text{pH}_{\text{fin}})$ difference as a function of the $\text{pH}_{\text{initial}}$ of the solution is shown in Figure 5. The pH at the point of zero charge (pH_{pzc}) was identified at about 7.5 (Figure 5). When the pH of the solution is lower than pH_{pzc} , the adsorption of the anionic species such as HCrO_4^- is favored whereas at pH values above the pH_{pzc} , the adsorption of the cationic elements predominates. (i) At $\text{pH} = 2$, the dominant form of chrome is HCrO_4^- . Thus, at low pH values, there is a large number of H^+ ions in the solution resulting in surface protonation of APTF, which leads to the formation of positively charged sites. These protons interact with the chromium species via electrostatic attraction forces thus HCrO_4^- is heavily adsorbed on the APTF surface. (ii) At $2 < \text{pH} < 6$, the progressive decrease in the adsorption rate is due to the coexistence of Cr_2O_7^- and CrO_4^- with HCrO_4^- causing competition on the

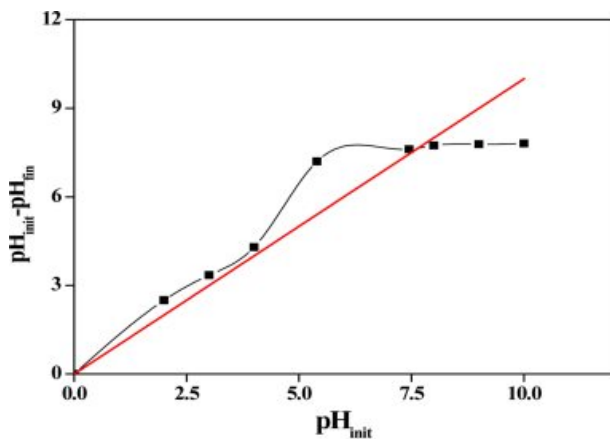


Figure 5. Determination of the point of zero charge.

adsorption sites. Similar results were reported in previous study.²⁴⁻²⁶ The decrease in Cr(VI) adsorption when the pH of the solution > 6 can be explained by the abundance of OH^- ions in solution, while the surface is negatively charged, which in turn initiates intensive electrostatic repulsion with the chromate and chromate hydrogen ions during the adsorption reaction.

Effect of Adsorbent Dose. The impact of the adsorbent dose on the removal efficiency of Cr(VI) from aqueous solution was explored by conducting several experiments using 100 mL solutions of Cr(VI) at initial concentration of 100 mg/L, at which different APTF amounts were charged at a temperature of 20 ± 1 °C and a stirring rate of 120 rpm while the contact time was 2 h and the corresponding results are revealed in Figure 6. First of all, the elimination of Cr(VI) was fast in the beginning of the adsorption process then the increase became slower until reaching a leveling off state.

It is apparent that the increase of the adsorbent dose was associated by elevation of the Cr(VI) adsorption level from 30% for 0.01 g to 95% for 0.2 g. This upturn is surely ascribed to the availability of larger number of adsorption sites by increasing the adsorbent dose.²⁷ In brief, the best possible adsorption efficiency was almost 85% and accomplished using 0.04 g of the adsorbent per 100 mL aqueous solution (0.4 g/L) for initial concentration dose 100 mg/L of Cr(VI).

Effect of Initial Cr(VI) Concentration. It is imperative that the high initial Cr(VI) presents a significant driving force to overcome the mass transfer resistance of ions moving from aqueous solution to a solid phase (adsorbent). This parameter was studied by formulating several Cr(VI) concentrations in the range from 100 to 300 mg/L while the APTF dose was

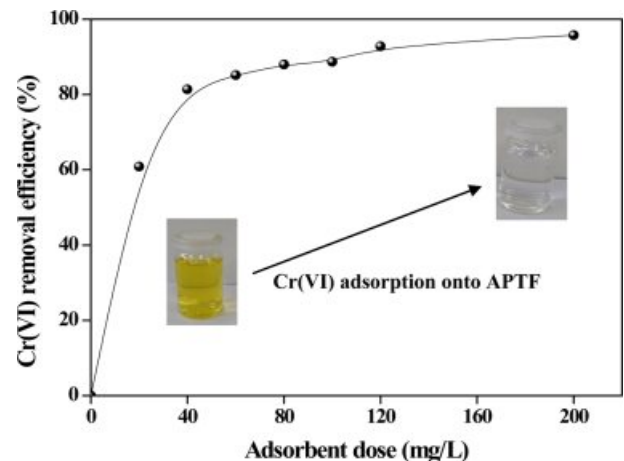


Figure 6. Variation of Cr(VI) adsorption onto APTF as a function of the adsorbent dose.

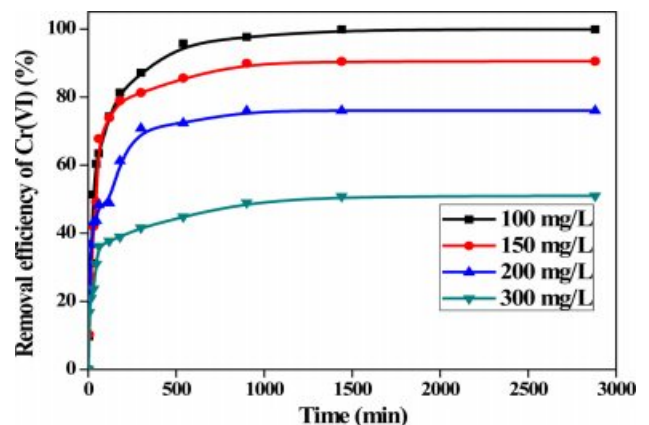


Figure 7. Variation of Cr(VI) removal (%) by APTF for different concentrations as a function of time.

kept unchanged. The development of chromium ions adsorption onto APTF as a function of time is illustrated in Figure 7. It can be dictated from Figure 7 that three phases are representing the mass transfer of Cr(VI) onto APTF. The first region is related to the external mass transfer effect. This is due to the initial availability of the free sites and the higher concentration of Cr(VI) ions, which provides strength to the ions to diffuse through the solution to the surface of the adsorbent. Then, the second region appears as expected to encounter a low adsorption rate as a result of the gradual decrease in the number of adsorption sites. Eventually, the third region is attributed to the low concentration gradient when the adsorption sites accomplished saturation thereby it remained constant. In our case, the adsorption was realized after 5 h and remained stable even after 48 h.

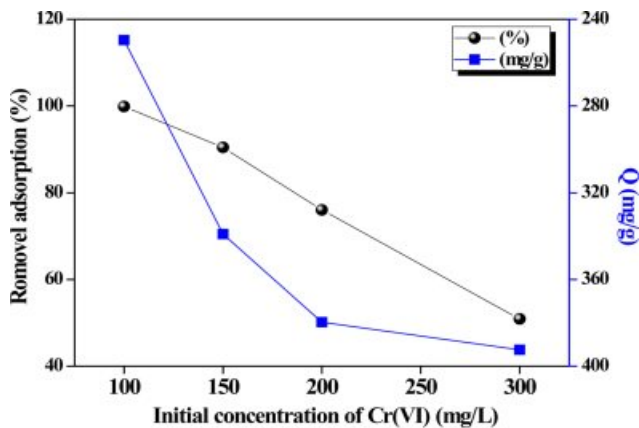


Figure 8. Variation of adsorption capacity and removal efficiency as a function of the initial Cr(VI) concentration.

Figure 8 shows the removal percentage of Cr(VI) along with the equilibrium adsorption capacity q_e of Cr(VI) on APTF as a function of the initial concentration of Cr(VI). This was achieved by feeding 0.4 g of APTF to 100 mL solutions of Cr(VI) incorporating various initial concentrations in the range 50-300 mg/L at pH \sim 2 and 20 °C. The results gave rise to the fact that the removal efficiency of Cr(VI) (%) collapses with the increase in the initial concentration of Cr(VI) as high concentration of Cr(VI) leads to the saturation of the adsorption sites of the APTF adsorbent, while the adsorption capacity, which is the amount of Cr(VI) adsorbed per unit mass of the adsorbent, q_e , behaves in a different way and increases in parallel with the increase in the initial concentration of Cr(VI). It was found that the Cr(VI) adsorption capacity by APTF increases without reaching a constant value for 300 mg/L while the removal efficiency decreased from 100% to 43% for increasing the initial concentration of Cr(VI) from 100 to 300 mg/L, respectively. The Cr(VI) removal was higher due to the accessibility of unoccupied binding sites on the APTF hence Cr(VI) ions are adsorbed rapidly onto the surface. In contrast, at high concentrations the ratio is low and the Cr(VI) removal percentage becomes small as most of the adsorption sites became engaged and not available any longer.

Adsorption Isotherm. The study of adsorption isotherm provides a good tool to explain the interaction of the adsorbate with the surface of the adsorbent. In this study, three isotherm models are investigated for this purpose; Langmuir, Freundlich and Dubinin-Radushkevich.²⁸ We focus in this study on two parameters in order to identify the most suitable isotherm that fits well to the relation between the adsorbate and adsorbent based on the correlation coefficient (R^2) and the APE means

(%). The correlation coefficient R^2 is described by eq. (3):

$$R^2 = \frac{\sum (q_m - q_e)^2}{\sum (q_m - q_e)^2 + \sum (q_m - q_e)^2} \quad (3)$$

Where, q_m : Maximum adsorption capacity (mg g⁻¹).

q_e : Average adsorption capacity (mg g⁻¹):

q_c : Equilibrium adsorption capacity (mg g⁻¹).

The APE(%) means used to ensure the reliability between experimental and theoretical values. It is expressed according to eq. (4):

$$\text{APE}(\%) = \frac{\sum_{i=0}^N |(q_e)_{\text{experimental}} - (q_e)_{\text{predicted}}| / (q_e)_{\text{experimental}}}{N} \times 100 \quad (4)$$

Where N is the number of experimental data.

The Langmuir model is applicable in cases of monolayer adsorption on a homogeneous surface containing a finite number of adsorption sites without interaction between the adsorbed molecules.²⁹ The Langmuir isothermal model is given by eq. (5):

$$\frac{C_e}{q_e} = \frac{1}{bQ_0} + \frac{C_e}{Q_0} \quad (5)$$

Where, C_e is the equilibrium concentration (mg/L) and q_e is the adsorption capacity at equilibrium (mg/g). The constant Q_0 (mg /g) represents the monolayer adsorption capacity while b is related to the heat of adsorption. R_L is a dimensionless constant called separation factor that can predict whether an adsorption system is favorable or not. R_L is calculated using the eq. (6)

$$R_L = \frac{1}{1 + bC_0} \quad (6)$$

Where C_0 is the initial concentration (mg/L). The favorability of the adsorption process by R_L parameter can be described as follows: For $R_L > 1$, the adsorption is unfavorable whereas in case of $0 < R_L < 1$, the adsorption has high favorability. Otherwise, $R_L=0$, signifies irreversible adsorption and $R_L=1$ reveals linear adsorption.

Moreover, the Freundlich isotherm model expresses the heterogeneous surface energies by multilayer adsorption and is expressed by the linear form in eq. (7):

Table 1. Parameters of the Langmuir, Freundlich and Dubinin-Radushkevich Isotherm Models

Models	Parameters	Values
Langmuir model	$q_m L$ (mg/g)	400
	K_L (L/mg)	0.5952
	R^2	0.9990
	APE(%)	5.56
Freundlich model	K_F (L/mg)	10.83
	R^2	0.9007
	n	9.11
	APE(%)	6.093
Dubinin-Radushkevich model	$q_m D$ (mg/g)	374.09
	R^2	0.9491
	b	$4 \cdot 10^{-7}$
	APE(%)	12.96

$$\ln q_e = \ln K_F + \left(\frac{1}{n}\right) \ln C_e \tag{7}$$

Where K_F (mg/g) is an indicator of the adsorption capacity and $1/n$ is the intensity of the adsorption presents indication of the adsorption favorability. Therefore, $n > 1$ means favorable adsorption conditions.

The Dubinin-Radushkevich model was also used to determine the porosity apparent free energy and the adsorption behavior.²⁹ The isothermal model of Dubinin-Radushkevich is given by the eq. (8)

$$\ln q_e = \ln q_s - B \varepsilon^2 \tag{8}$$

Where q_s is the theoretical saturation capacity, B is a constant related to the biosorption energy and ε is the Polanyi potential that can be calculated according to eq. (9):

$$\varepsilon = RT \ln \left(1 + \frac{1}{C_e}\right) \tag{9}$$

Where C_e is the equilibrium concentration (mg/L); $R = 8.314$ J/mol and T is the absolute temperature ($^{\circ}K$). The isotherm parameters were calculated from the linear plots and are summarized in Table 1. Additionally, all data of the different isotherm models are exhibited in Figure 9(a), 9(b) and 9(c), respectively. Based on the R^2 values and the APE means, the results of Cr(VI) adsorption on APTF are best correlated to the Langmuir isotherm ($R^2 > 0.999$) indicating a monolayer adsorption of Cr(VI) ions on the surface of the adsorbent via electrostatic attraction forces.

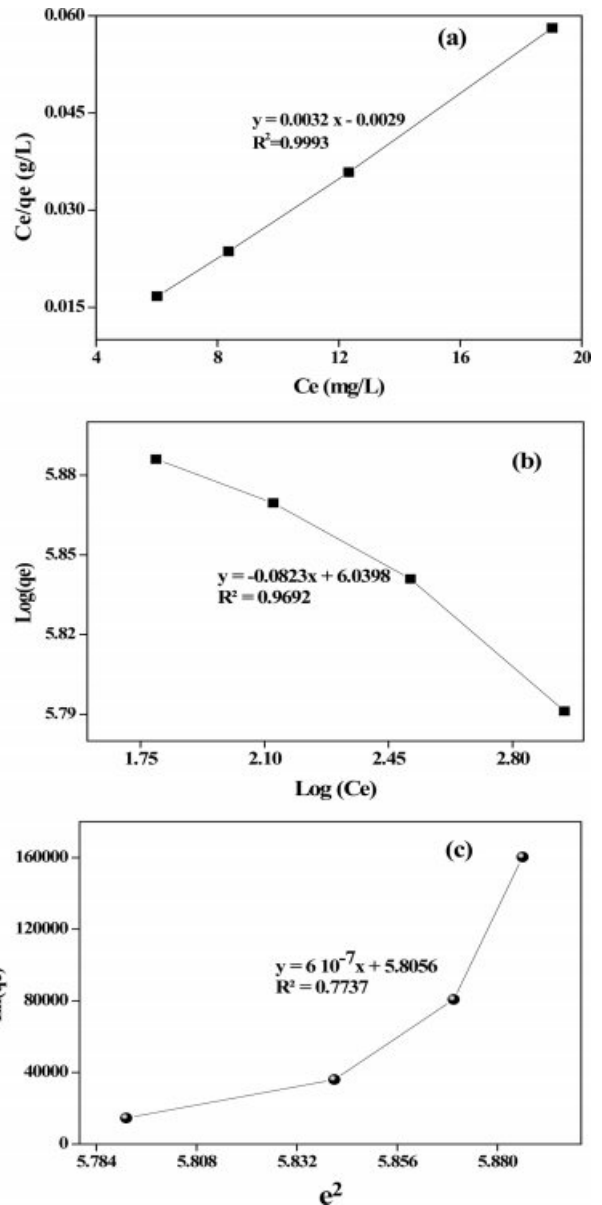


Figure 9. Adsorption isotherm profiles: (a) Langmuir; (b) Freundlich; (c) Dubinin-Radushkevich.

The obtained maximum adsorption capacity, $q_{mL} = 400$ mg/g and the Langmuir K_L constant (0.5952 L/mg) are also suggesting that the adsorption of Cr(VI) onto APTF proceeds as a single layer, which corroborates a homogenous surface of adsorbent as well. Moreover, the R_L indicates an irreversible favorable adsorption is taking place. Further, the value of $1/n$, which is ranged from 0 to 1 signifies a high adsorption intensity.

Adsorption Kinetics. Kinetic parameters are suitable means for predicting important information about the adsorption process. So 0.04 g of APTF was immersed in 100 mL of Cr(VI)

Table 2. Parameters of Pseudo First Order, Pseudo Second Order and Intra-particle Diffusion Kinetic Models

Cr(VI) mg/L	Pseudo first order Model				Pseudo second order			Intra-particle diffusion		
	q (exp)	R^2	$K_1(10^4)$	$q(\text{cal})$	R^2	K_2	$q(\text{cal})$	k_{diff}	R^2	$q(\text{cal})$
100	245.5	0.9156	1.059	132.91	0.9998	1.394	250	1.040	0.9927	194.93
150	344	0.9210	1.151	192.02	0.9998	0.929	344.18	0.740	0.9794	240.96
200	379.99	0.9398	1.704	259.61	0.9997	1.115	384.61	0.990	0.9620	461.46
300	392.5	0.8122	1.243	131.34	0.9990	2.224	400	3.650	0.9870	213.95

Table 3. Comparison between the Adsorption Capacities of Various Tannin Adsorbents and Our “APTF” for Cr(VI) Removal

Adsorbents	Maximum adsorption capacity (mg/g)	Adsorbent dose (g/L)	References
Poly(tannin-hexamethyldiamine)	283.29	0.5	Q. Liu <i>et al.</i> ³²
Persimmon tannin gel	287.040	0.2	Nakajima and Baba ¹¹
Tannin-nanocellulose composite	103.259	0.5	Q. Xu <i>et al.</i> ¹⁰
Tannin gel	287	2.5	Y. Nakano <i>et al.</i> ¹²
Persimmon tannins immobilized on collagen	49.01	0.1	J. Cui <i>et al.</i> ³³
Quebracho tannin resins	83.33	1	M. Yurtsever <i>et al.</i> ³⁴
APTF	370	0.4	This study

solutions (0.4 g/L) possessing different initial concentrations ranging from 100 to 300 mg/L at pH = 2 and 20 °C. The adsorption kinetics can be explained as the solute removal rate that controls how long the adsorbate stays at the solid-liquid interface.³⁰ This part was achieved to verify the mechanism of Cr(VI) ions adsorption into APTF. The kinetics have been fitted to different models such as the pseudo-first order, pseudo-second order and the intra-particle models,³¹ which are represented by eqs. (10), (11), and (12), respectively:

$$\log(q_e - q_t) = \log q_e - \frac{K_1}{2.303} t \quad (10)$$

$$\frac{t}{q_t} = \frac{1}{K_2 q_e^2} + \frac{1}{q_e} t \quad (11)$$

$$\frac{1}{q_e - q_t} = \frac{1}{q_e} + K_2 t \quad (12)$$

$$q_t = k_{\text{diff}} \times t^{0.5} + C^* \quad (13)$$

where q_e and q_t are the amounts of Cr(VI) ions (mg/g) adsorbed at equilibrium and at time t , respectively; K_1 and K_2 are the rate constant of the pseudo-first order and the pseudo-second order rate constant, respectively; and t (min) is the contact time, k_{diff} ($\text{mg g}^{-1} \text{mn}^{-0.5}$) is the intra-particle diffusion rate constant and C is the intercept. The kinetic parameters K_1 , K_2 , k_{diff} , q_e , q_t , C together with R^2 are collected in Table 2.

Based on the values of R^2 obtained from different models, it

can be decided that the data follow the pseudo second order model as its R^2 (0.9998) is closer to unity and the experimental adsorption capacity is the nearest to the theoretical one. Hence, the rate constant obtained by applying the pseudo-second order model was 1.39×10^{-4} . The maximum adsorption capacity (Q_{max}) for Cr(VI) onto APTF was compared with those reported in the literature as shown in Table 3. It can be noted from the table that the obtained Q_{max} in this study is higher when compared with most recently reported tannin based adsorbents.^{10-12,32-34} This finding indicates that the applied foam in this study, which is formulated from pinus halpensis tannin, is a better alternative to many other adsorbents especially considering the price perspective.

Thermodynamic Parameters. Thermodynamic parameters such as enthalpy ΔH (kJ/mol), standard entropy ΔS (J/mol K) and Gibbs free energy variations ΔG (kJ/mol) were calculated using eqs. (14)-(17) in order to understand the adsorption process more intensely. Figure 10 illustrates the variation of K_c as a function of $1/T$. The thermodynamic parameters (T , ΔG° , ΔH° and ΔS°) for the adsorption of Cr (VI) by APTF are calculated at different temperatures as demonstrated in Table 4.

$$K_c = \frac{C_0 - C_e}{C_e} \quad (14)$$

$$\ln K_c = -\frac{\Delta H}{RT} + \frac{\Delta S}{R} \quad (15)$$

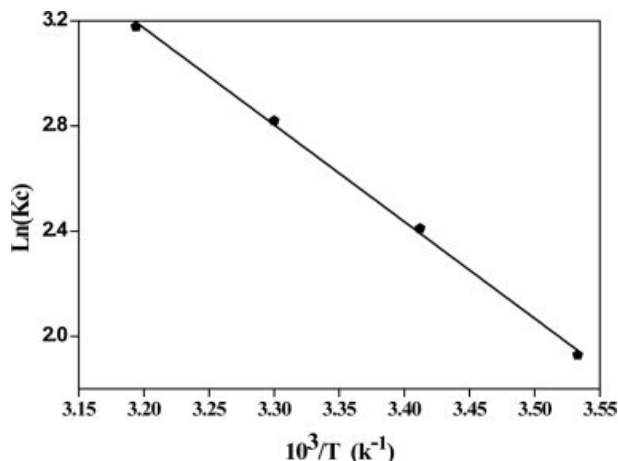


Figure 10. $\ln(K_c)$ versus $1/T$ plot.

Table 4. Thermodynamic Parameters for the Adsorption of Cr(VI) by APTF at Different Temperatures

T (K)	ΔG° (KJ/ mol)	ΔH° (kJ/mol)	ΔS° (J/mol K)
293	-4.608		
303	-5.852		
313	-7.097	30.614	124.46
323	-8.341		

$$\Delta G = -RT \ln K_c \quad (16)$$

$$\Delta G = \Delta H - \Delta S \quad (17)$$

Where K_c is the equilibrium constant, C_e and C_0 are the equilibrium and initial concentrations for Cr(VI) adsorption on APTF (mg/L), respectively, R is a universal gas constant (8.314 J/K mol) and T is the absolute temperature (K).

From Figure 11, it is clear that the adsorption capacity by the adsorbent enhances with increasing the temperature. This performance can be explained by the increased molecular movement, which causes weakening of the hydrogen bonds formed between the water molecules and the solute, thereby increasing diffusion to the pores. As a result, the positive value of the enthalpy ΔH° (30.614 kJ/mol) proves the endothermic nature of the adsorption reaction. Furthermore, the positive value of ΔS° (124.46 J/mol.K) also suggests good affinity of the Cr(VI) ions to the adsorbent and the high randomness at the solid-liquid interface during the binding of the metal ion onto the active sites of the adsorbent. The categorization of the adsorption reaction as favorable and spontaneous was verified from the negative values of ΔG° . As an example, the increase in tem-

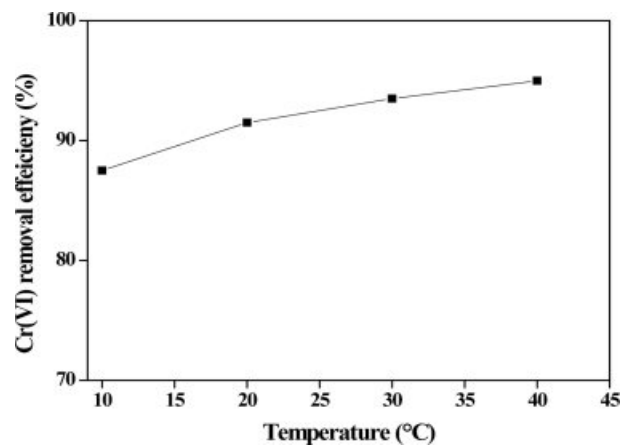


Figure 11. Cr(VI) adsorption onto APTF as a function of temperature.

perature from 20 to 40 °C was accompanied by a change in the ΔG value from 4.608 to 8.341 kJ/mol. The thermodynamic parameters for the adsorption process of Cr(VI) onto APTF are matching well with those reported in the literature.^{24,35,36}

Conclusions

An efficient adsorbent was formulated mainly from Algerian natural pinus halepensis tannin (APTF). Various characterizations performed on this adsorbent indicated its promise in water purification. Thus, adsorption results revealed it was very efficient in the removal of Cr(VI) ions from aqueous solutions with a maximum adsorption capacity around 390 mg g⁻¹ at pH ~ 2, which was mostly attributed to the contribution of -OH functional group in interaction with chromium ions. The rate limiting step for the adsorption process was best fitted with pseudo-second order kinetic model for the studied concentrations (100-300 mgL⁻¹). Agreeable correlation for Cr(VI) adsorption to the adsorbent was found with a single-layer adsorption capacity of 400 mg g⁻¹ at 20 °C as signified by the Langmuir isotherm model. The adsorption process could be classified mainly as chemical ion exchange as concluded from the average free energy values estimated from the Dubinin-Radushkevich model. The negative values of free Gibbs energy (ΔG°) and positive enthalpy (ΔH°) designated the spontaneous and endothermic features of the adsorption process for the different temperatures examined. The positive value of entropy (ΔS°) clearly reflected the increased randomness at the solid-solution interface through the adsorption of Cr(VI) onto the foam. Based on these facts, it can be ensured that APTF is an efficient adsorbent and can be suc-

cessfully employed for the adsorption of Cr(VI) ions from aqueous solutions for the purpose of water purification.

Acknowledgements: Authors acknowledge the financial support provided by DGSRTD, URA-DTE and CRAPC.

References

- H. E. Muga and J. R. Mihelcic, *J. Environ. Manage.*, **88**, 437 (2008).
- D. Paustenbach, B. Finley, F. Mowat, and B. Kerger, *J. Toxicol. Environ. Health A*, **66**, 1295 (2003).
- H. A. M. Bacelo, S. C. R. Santos, and C. M. S. Botelho, *Chem. Eng. J.*, **303**, 575 (2016).
- R. Fan, F. Xie, X. Guan, Q. Zhang, and Z. Luo, *Bioresour. Technol.*, **163**, 167 (2014).
- G. Tondi, C. W. Oo, A. Pizzi, A. Trosa, and M. F. Thevenon, *Ind. Crops Prod.*, **29**, 336 (2009).
- J. Sánchez-Martín, J. Beltrán-Heredia, and P. Gibello-Pérez, *Chem. Eng. J.*, **168**, 1241 (2011).
- J. Sánchez-Martín, M. González-Velasco, and J. Beltrán-Heredia, *J. Wood Chem. Technol.*, **29**, 119 (2009).
- J. Beltrán-Heredia, J. Sánchez-Martín, and C. Gómez-Muñoz, *Appl. Water Sci.*, **2**, 199 (2012).
- G. Tondi and A. Pizzi, *Ind. Crops Prod.*, **29**, 356 (2009).
- Q. Xu, Y. Wang, L. Jin, Y. Wang, and M. Qin, *J. Hazard. Mater.*, **339**, 91 (2017).
- A. Nakajima and Y. Baba, *Water Res.*, **38**, 2859 (2004).
- Y. Nakano, K. Takeshita, and T. Tsutsumi, *Water Res.*, **35**, 496 (2001).
- J. Hassoune, S. Tahiri, M. El Krati, M. L. Cervera, and M. de la Guardia, *J. Environ. Eng.*, **144**, 04018060 (2018).
- A. Celzard, W. Zhao, A. Pizzi, and V. Fierro, *Mater. Sci. Eng. A*, **527**, 4438 (2010).
- N. Kadri, B. Khettal, Y. Aid, S. Kherfellah, W. Sobhi, and V. Brragan-Montero, *Food Chem.*, **188**, 184 (2015).
- N. E. Meikleham and A. Pizzi, *J. Appl. Polym. Sci.*, **53**, 1547 (1994).
- L. Chupin, C. Motillon, F. Charrier-El Bouhtoury, A. Pizzi, and B. Charrier, *Ind. Crops Prod.*, **49**, 897 (2013).
- C. Lacoste, A. Pizzi, M.-C. Basso, M.-P. Laborie, and A. Celzard, *Ind. Crops Prod.*, **52**, 450 (2014).
- M. V. Lopez-Ramon, F. Stoeckli, C. Moreno-Castilla, and F. Carrasco-Marin, *Carbon*, **37**, 1215 (1999).
- A. Moubarik, A. Pizzi, A. Allal, F. Charrier, and B. Charrier, *Ind. Crops Prod.*, **30**, 188 (2009).
- H. Saad, A. Khoukh, N. Ayed, B. Charrier, and F. C.-E. Bouhtoury, *Ind. Crops Prod.*, **61**, 517 (2014).
- G. Tondi and A. Petutschnigg, *Ind. Crops Prod.*, **65**, 422 (2015).
- G. Vázquez, E. Fontenla, J. Santos, M. S. Freire, J. González-Álvarez, and G. Antorrena, *Ind. Crops Prod.*, **28**, 279 (2008).
- R. Labied, O. Benturki, A. Y. Eddine Hamitouche, and A. Donnot, *Adsorpt. Sci. Technol.*, **36**, 1066 (2018).
- M. Rao, A. V. Parwate, and A. G. Bhole, *Waste Manage.*, **22**, 821 (2002).
- H. Uzun, Y. K. Bayhan, Y. Kaya, A. Cakici, and O. F. Algur, *Bioresour. Technol.*, **85**, 155 (2002).
- J. Yang, M. Yu, and W. Chen, *J. Ind. Eng. Chem.*, **21**, 414 (2015).
- E. I. Unuabonah, M. O. Omorogie, and N. A. Oladoja, "Modeling in Adsorption: Fundamentals and Applications", in *Composites Nanoadsorbents*, G. Z. Kyzas and A. C. Mitropoulos, Editors, Elsevier, p 85 (2019).
- S. Karnjanakom and P. Maneechakr, *J. Mol. Struct.*, **1186**, 80 (2019).
- P. K. Pandey, S. K. Sharma, and S. S. Sambhi, *Int. J. Environ. Sci. Technol.*, **7**, 395 (2010).
- A. Olad and F. F. Azhar, *Desalin. Water Treat.*, **52**, 2548 (2014).
- Q. Liu, Q. Liu, B. Liu, T. Hu, W. Liu, and J. Yao, *J. Hazard. Mater.*, **352**, 27 (2018).
- J. Cui, Z. M. Wang, F. L. Liu, P. B. Dai, R. Chen, and H. Y. Zhou, *Mater. Sci. Forum*, **743-744**, 523 (2013).
- M. Yurtsever and İ. A. Şengil, *J. Hazard. Mater.*, **163**, 58 (2009).
- R. Khosravi, G. Moussavi, M. T. Ghaneian, M. H. Ehrampoush, B. Barikbin, A. A. Ebrahimi, and G. Sharifzadeh, *J. Mol. Liq.*, **256**, 163 (2018).
- R. Saha, K. Mukherjee, I. Saha, A. Ghosh, S. K. Ghosh, and B. Saha, *Res. Chem. Intermed.*, **39**, 2245 (2013).